JOURNAL OF THERMOPHYSICS AND HEAT TRANSFER
Vol. 22, No. 2, April–June 2008

Studies of Chemi-Ionization and Chemiluminescence in Supersonic Flows of Combustion Products

Saurabh Keshav,* Yurii G. Utkin, Munetake Nishihara, Ainan Bao, J. William Rich, and Igor V. Adamovich
The Ohio State University, Columbus, Ohio 43210

DOI: 10.2514/1.30822

A stable ethylene/oxygen/argon flame is sustained and nearly complete combustion is achieved in the combustion chamber of an $M = 3$ supersonic nozzle, at a stagnation pressure of $P_0 = 1$ atm. Ultraviolet and visible emission is detected both from the combustion chamber and from the $M = 3$ flow of combustion products. Temperature in the combustor, inferred from the visible emission spectra, is $T_0 = 2000 \pm 200$ K. Electron density in $M = 3$ flow of combustion products has been measured using Thomson discharge $n_e = 1.4 \pm 0.2 \cdot 10^8$ cm^{-3}, at an ionization fraction of $n_e/N = (0.65 \pm 0.15) \cdot 10^{-9}$. This corresponds to an electron density of $n_{e0} = 2.2 \cdot 10^9$ cm^{-3} in the combustor. The chemi-ionization current measured in the $M = 3$ flow is found to be proportional to the equivalence ratio in the combustor. The time-resolved chemi-ionization current is in very good correlation with the visible emission from ethylene–air and propane–oxygen–argon flames in the combustor at unstable combustion conditions. The results show that nearly all electrons can be removed from the supersonic flow of combustion products by applying a moderate transverse electric field. No effect of electron removal on visible emission has been detected. A similar result was obtained for nitric oxide β bands and cyanogen violet band emission, when nitric oxide was injected into the combustion product flow.

Nomenclature

A	=	electrode surface area
A_{cross}	=	supersonic test section cross-sectional area
A^*	=	nozzle throat area
D_e, D_i	=	electron and ion diffusion coefficients
e	=	electron charge
h	=	distance between the electrodes in the supersonic test section
I_e	=	current between the electrodes
I_s	=	spark plug current
I_{sat}	=	chemi-ionization saturation current
L	=	length of computational domain
l	=	nozzle length
M	=	Mach number
N	=	number density in the test section
n_e	=	electron density in the test section
n_{e0}	=	electron density in the combustor
n_i	=	ion density in the test section
P_{back}	=	vacuum tank pressure
P_0	=	combustor/plenum pressure
P_1	=	static pressure at nozzle exit
P_2	=	static pressure at diffuser inlet
R	=	gas constant
R_e	=	electrode ballast resistor
R_s	=	spark plug ballast resistor
S	=	electron flux through the test section
T	=	test section temperature
T_{ad}	=	adiabatic flame temperature
T_0	=	combustor/plenum temperature
U_e	=	voltage between the electrodes
U_{PS}	=	spark plug power supply voltage
U_s	=	voltage across the spark plugs
U_{sat}	=	saturation voltage
u	=	flow velocity in combustor
u_{flow}	=	test section flow velocity
β_{ei}	=	electron-ion recombination rate
γ	=	specific heat ratio
ε_0	=	dielectric permeability of vacuum
μ_e, μ_i	=	electron and ion mobilities
τ_{rec}	=	characteristic electron recombination time
τ_{flow}	=	flow residence time
Φ	=	equivalence ratio

Presented as Paper 1353 at the 45th Aerospace Sciences Meeting and Exhibit, Reno, NV, 8–11 January 2007; received 4 March 2007; revision received 13 July 2007; accepted for publication 13 July 2007.

*Nonequilibrium Thermodynamics Laboratories, Department of Mechanical Engineering.

I. Introduction

SPECTRAL characteristics of high-altitude rocket plume signatures are of great importance for detection, identification, and tracking of missiles [1–4]. Insight into the UV/visible plume signatures, and possibly control of plume emission, require understanding of energy transfer mechanisms among the excited species in plume flows. Specifically, identification of energy transfer processes generating radiating species and determining the rates of these processes are among key technical issues. Missile launch experiments [1,5,6] demonstrated that emission from rocket plumes, such as CO fourth positive bands [1], may persist over anomalously long periods of time after the engine cutoff. This suggests that short-lived radiating species, such as CO($A^1\Pi$) (radiative lifetime of $\sim$10 ns), may be created by energy transfer from long-lived, metastable "dark species," which may store energy for a long time.

An example of such energy storage in metastable species, with subsequent energy transfer to radiating species producing UV/visible emission, has been studied in recent CO optical pumping experiments [7,8]. In these experiments, nonequilibrium low-temperature plasma is created by resonance absorption of a continuous wave (cw) CO laser radiation by CO-Ar and CO-N_2 mixtures with additives such as NO in a flowing absorption cell. High CO vibrational levels (up to $v \sim 40$), which are not directly coupled to the laser radiation, are excited by collisional vibration–vibration energy (V–V) exchange:

$$\text{CO}(v) + \text{CO}(w) \rightarrow \text{CO}(v-1) + \text{CO}(w+1) \qquad v, w \sim 0\text{–}40 \tag{1}$$

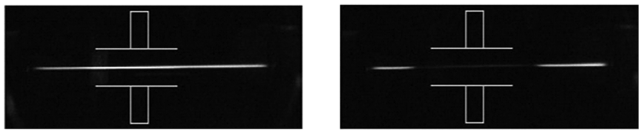

Fig. 1 Photographs of CO-N_2 optically pumped plasmas [7]. The location of Thomson electrodes is highlighted. Left, no voltage applied (electrons present); right, 2 kV voltage applied (electrons removed).

Typical CO vibrational temperature at these conditions is $T_v = 3000$–4000 K, with up to 40 vibrational levels populated, whereas the translational/rotational temperature remains rather low, $T = 300$–700 K [7,9]. At these extremely nonequilibrium conditions, ionization occurs in collisions of two highly vibrationally excited molecules, by associative ionization mechanism [10–12],

$$\mathrm{CO}\,(v) + \mathrm{CO}(w) \rightarrow (\mathrm{CO_2})^+ + e^- \tag{2}$$

These optically pumped CO-Ar-N_2-NO plasmas generate UV/visible emission from electronically excited species, C_2 (Swan bands), CO (fourth positive system bands), CN violet system, and NO β and γ bands [7,8]. Optical pumping studies of the UV/visible emission mechanism showed that removing electrons from the plasma by applying a moderate dc electric field results in dramatic reduction of the UV/visible emission [7,8]. This method of electron removal from the plasma is known as Thomson discharge [10]. Figure 1 shows photographs of visible emission from the optically excited CO-N_2 plasma, with and without electrons present in the plasma [7]. When the electrons are removed from the plasma, the C_2 Swan and CN violet band emission decreases by up to 80–90%, so that the plasma glow nearly disappears (see Fig. 1). This effect is detected at ionization fractions as low as $n_e/N \sim 10^{-9}$. A similar effect was detected for CO fourth positive bands as well as for NO β and γ bands. These results demonstrated that low-energy electrons mediate energy transfer from vibrationally excited CO molecules (metastable "dark" states) to excited electronic levels, via superelastic electron-molecule collisions followed by electron impact excitation of radiating electronic states of molecules [7,8].

The radiating species detected in the optically pumped plasmas, such as CO($A^1\Pi$), NO($A^2\Sigma$), and NO($B^2\Pi$) are among the species that produce UV/visible emission in rocket plumes [1]. Also, it is well known that high-temperature combustion product flows, such as those occurring in chemical rocket engines, are ionized due to chemi-ionization [13–16]. This suggests that a similar energy transfer process from metastable to radiating species, mediated by electrons, may contribute to UV/visible emission of combustion products in plumes. At these conditions, however, vibrational excitation is unlikely to be a factor because vibrational relaxation time in high-temperature flows in the presence of hydrocarbons and water vapor is very short. On the other hand, electronically excited metastable molecules, such as $N_2(A^3\Sigma)$ or CO($a^3\Pi$), may be among the relatively long-lived, energy-storing species. Therefore, studies of possible coupling of chemi-ionization and chemiluminescence in combustion product flows may provide insight into the plume emission mechanisms.

There is considerable literature on the vacuum ultraviolet (VUV)/UV emission and chemi-ionization mechanisms in hydrocarbon flames (e.g., see [17–27]), which includes studies of CO fourth positive system, OH 306.4 nm system, and CH 430 nm system emission. Some results [20,21,25] show similarities between the two processes. In particular, it has been suggested [25] that both chemi-ions and electronically excited OH($A^2\Sigma^+$) molecules may have the same precursor, CH radical. This indicates that chemi-ionization and chemiluminescence processes may be coupled, although direct experimental evidence on such coupling is not available. Therefore, controlling the number density of electrons and ions generated by chemi-ionization processes in combustion flows (e.g., by applying electric field across the flow) may help control UV/visible chemiluminescence emission, such as that which has been done in optically pumped plasmas [7,8].

Additional motivation for studies of chemiluminescence and chemi-ionization in combustion product flows is combustion sensing and control. Previous experiments in hydrocarbon flames showed that the emission intensity ratio at fuel-lean conditions, $I_{\mathrm{CH}^*}/I_{\mathrm{OH}^*}$, varies almost linearly with the equivalence ratio [28]. Feasibility of feedback combustion control using chemiluminescence has been demonstrated in recent experiments in hydrocarbon flames, where the OH 306.4 nm band emission signal was monitored and the equivalence ratio was controlled by adding fuel to the combustor when the emission signal decreased [29]. However, the accuracy of optical sensing may be affected by optical thickness of the flame and soot deposits on the collecting optics. On the other hand, chemi-ionization current measurement is simple to implement and interpret. Indeed, previous experimental work shows that chemi-ionization current is directly related to the equivalence ratio in the combustor [30,31]. Such a relationship suggests that chemi-ionization current can be used to monitor the equivalence ratio in the combustor, and possibly to control it by using a feedback loop.

The main objectives of the present paper are 1) to detect chemiluminescence in supersonic flows of hydrocarbon combustion products using UV/visible emission spectroscopy, 2) to measure electron density in these flows, 3) to detect correlation between the electron density in the flow and the conditions in the combustor, and 4) to determine whether electron removal from the flow affects UV/visible emission intensity.

II. Experimental

Figure 2 shows a schematic of the experimental apparatus, which consists of a combustion chamber followed by a converging–diverging nozzle and a supersonic test section through which combustion products exhaust into the vacuum system. Oxidizer (dry air or a 20%O_2-80%Ar mixture) enters a combustion chamber through a 1 in. delivery line connected to the backplate of the test section, as shown in Figs. 2 and 3. The fuel (ethylene or propane) is delivered through a 1/4 in. line and injected into the combustor through a choked injection port 1 mm in diameter. Both the oxidizer and the fuel flows, supplied from gas cylinders, are choked using pinhole sonic choke plates inserted into the oxidizer and fuel delivery lines. The pinhole diameters are 4.5 mm (in the oxidizer line) and 1.0 mm (in the fuel line). At the present conditions, the minimum pressure ratio across the choke plates is 2.2 for the oxidizer flow and 2.5 for the fuel flow.

The pressure in the combustor is measured using a wall pressure tap shown in Fig. 2. For emission spectroscopy measurements, the combustor is equipped with two rectangular optical access windows made of magnesium fluoride, flush in the side walls. The combustion chamber also acts as a plenum of the aerodynamically contoured $M = 3$ nozzle. The side walls of the nozzle are the contoured walls. The nozzle height remains constant, $h = 1$ cm, in the subsonic part up to the throat. The nozzle throat cross section is $A^* = 1 \times 0.82$ cm. Downstream of the throat, the top and the bottom walls are diverging at 1 deg angle each to provide boundary-layer relief. The subsonic area ratio of the nozzle $A/A^* = 6.1$ corresponds to the combustor Mach number of $M = 0.09$ (flow velocity $u = 30$ m/s at $T_0 = 300$ K and $u = 80$ m/s at $T_0 = 2000$ K). Therefore, the combustor pressure is close to the flow stagnation pressure. The fuel and oxidizer mass flow rates are measured using their pressures upstream of the choke plates in the delivery lines:

$$\dot{m} = P_0 A^* \sqrt{\frac{\gamma}{T_0 R}\left(\frac{2}{\gamma+1}\right)^{\frac{\gamma+1}{\gamma-1}}} \tag{3}$$

Because the flows in the oxidizer and fuel delivery lines remain choked during the entire experiment, their mass flow rates also remain the same after ignition, which is critical for combustion stability. Equation (3) has also been used to measure the flow rate of the mixture through the combustor, in which case P_0 and T_0 are the combustor/plenum pressure and temperature, and A^* is the nozzle throat area. In that case, the fractions of fuel and oxidizer in the

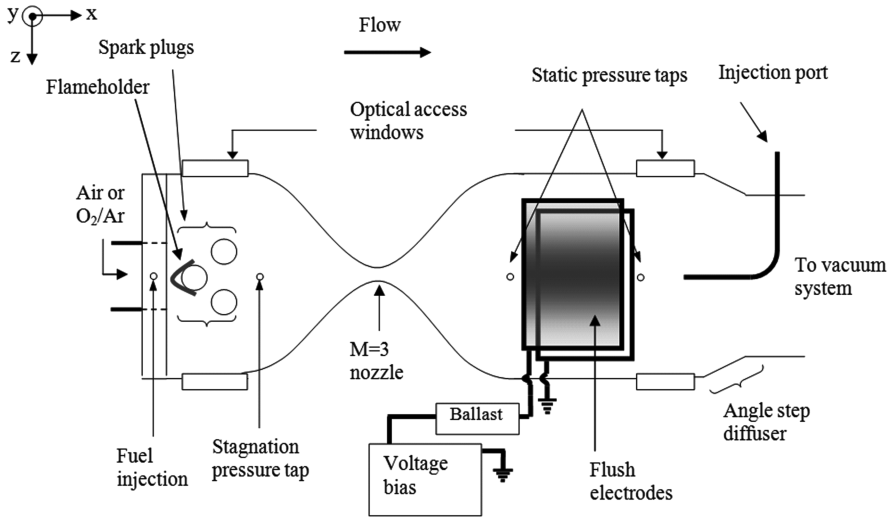

Fig. 2 Schematic of experimental setup.

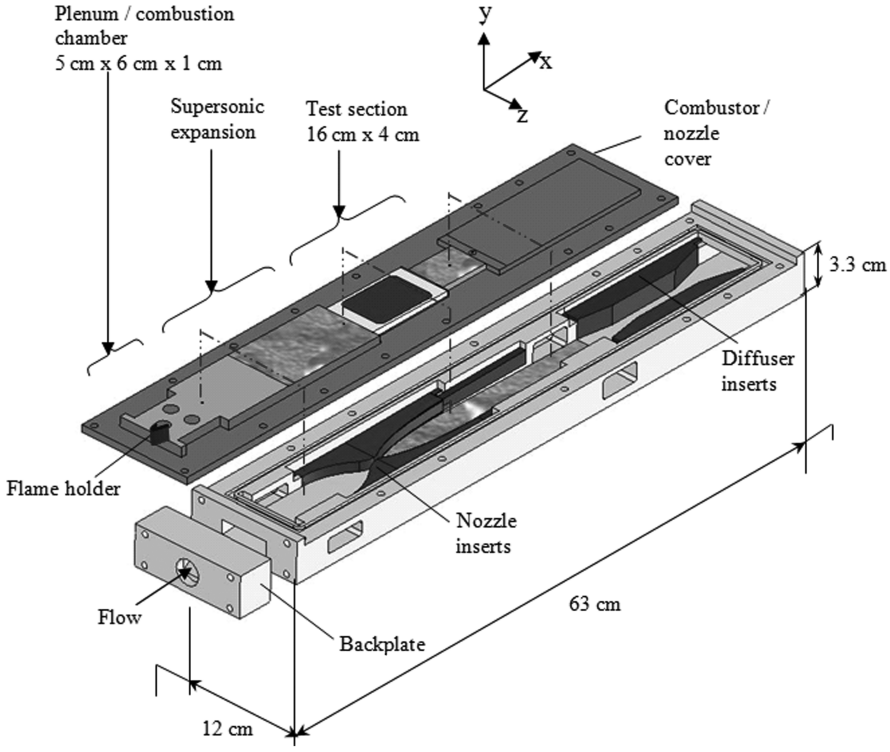

Fig. 3 Overall view of the combustor/nozzle/test section/diffuser assembly.

mixture have been determined by measuring their partial pressures in the plenum before ignition.

To ignite the fuel/oxidizer mixture, the combustion chamber has three spark plugs arranged in an isosceles triangle, as shown in Fig. 2, bolted to the combustor/nozzle cover plate. The fuel/oxidizer mixing occurred in the injection flow in the backplate 4-cm-thick upstream of the spark plugs, as shown in Fig. 2. The spark plugs are connected to a high-voltage dc power supply (Glassman, 5 kV, 2 A) and are individually ballasted ($R_s = 10$ kΩ). A V-shaped copper plate flame holder is bolted to the cover plate near the upstream spark plug, as shown in Fig. 2. The flame holder stabilizes the flame after the spark plugs are turned off. The dc power supply voltage applied to the spark plugs is typically $U_{PS} = 2$ kV in a $C_2H_4/O_2/Ar/$ mixture and $U_{PS} = 5$ kV in air/C_2H_4. After dc arc discharges are initiated in the spark plugs, the voltage across each spark plug is $U_s = U_{PS} - I_s R_s = 1$ kV at the current of $I_s = 100$ mA (in ethylene/oxygen/argon mixture).

Downstream of the nozzle is a rectangular cross section supersonic test section. The top and bottom walls of the test section continue to diverge at 1 deg angle each up to the diffuser inlet. Two static pressure ports are located in the top wall, 0.5 cm downstream of the nozzle exit and 4 cm upstream of the diffuser inlet, as shown in Fig. 2. The test section is equipped with two additional rectangular optical access magnesium fluoride windows and a rectangular copper electrode, 6.8 cm long and 4 cm wide, flush mounted in the top wall, as shown in Fig. 2. The electrode is insulated from the grounded test section using a mica ceramic housing and is used for chemi-ionization current and electron density measurements, as well as for electron removal from the supersonic flow. The grounded test section acts as the second electrode. The electrode can be biased to moderate voltages (up to a few hundred volts) using a separate low-current dc power supply (Thorn EMI 3000R, 0–3 kV, 0–5 mA). The electrode is connected to high-voltage output of the power supply through a ballast resistor $R_e = 0.7$ MΩ, as shown in Fig. 2. The current

between the electrode and the test section was determined by measuring the voltage drop on the ballast resistor using a Tektronix P6139A high-voltage probe. Typically, the voltage applied to the electrode is much lower than the breakdown voltage at the present conditions. Therefore, the applied voltage does not generate any charged species in addition to chemi-ionization of the flow in the combustor.

Downstream of the supersonic test section is an angle step diffuser. The $M = 3$ diffuser throat width is 3.0 cm, 75% of the test section width. The upstream and downstream step angles are 9 and 15 deg, respectively. The combustor/nozzle/test section/diffuser assembly is attached to a vacuum system connected to a 1200 ft^3 dump tank pumped out by an Allis-Chalmers 1900 cfm rotary vane vacuum pump. The minimum pressure in the vacuum system sustained by the pump is $P_{\text{back}} = 35$–40 torr, which necessitates the use of the diffuser with the test section operated at relatively low static pressures of $\sim$15 torr (at $P_0 \sim 1$ atm).

The entire assembly is machined from a single piece of steel with a steel cover plate and a separate backplate. The nozzle and the diffuser inserts are removable, which makes possible replacing an $M = 3$ nozzle with an $M = 4$ nozzle or adjusting diffuser geometry. Figure 3 shows the overall view of the test section. The flow direction in Fig. 3 is from left to right.

In the present experiment, optical diagnostics includes visible emission spectroscopy and infrared absorption spectroscopy. Visible emission signal from the combustor or from the supersonic test section was collected through the magnesium fluoride optical access windows and focused on the spectrometer slit using two fused silica plano-convex lenses (focal distance of 30.5 cm) and a gold-plated plane mirror. Optical emission spectra in the UV/visible range (250–800 nm) were taken using an optical multichannel analyzer (OMA) with a Spectra Physics 0.5 m monochromator with 1200 lines/mm grating and a Princeton Instruments intensified charge-coupled device (ICCD) array camera. In addition, time-resolved UV/visible emission intensity at different wavelengths was monitored using an Acton Research vacuum UV spectrometer (model VM 504) with a photomultiplier tube. Also, we used a Biorad 175C dynamic alignment Fourier transform infrared (FTIR) spectrometer with a liquid N_2 cooled In-Sb detector to determine combustion completeness and combustion product concentrations by infrared absorption spectroscopy. For this, combustion product flow was sampled into an absorption cell of the FTIR through a pitot probe 1.6 mm in diameter, inserted into the supersonic flow through one of the pressure ports, as shown in Fig. 2. The pitot probe was placed 13.5 cm downstream of the nozzle exit (2.5 cm upstream of the diffuser inlet).

III. Thomson Discharge Model

To model the electron removal from the flow by transverse electric field applied to the electrodes in the supersonic test section, we used a two-dimensional non-self-sustained dc discharge (Thomson discharge) model [32]. The model incorporates equations for the ion and for the electron densities in the decaying plasma, as well as the Poisson equation for the electric potential distribution:

$$\frac{\partial n_i}{\partial t} + \frac{\partial \Gamma_{i,x}}{\partial x} + \frac{\partial \Gamma_{i,y}}{\partial y} = -\beta_{ei} n_i n_e \tag{4}$$

$$\frac{\partial n_e}{\partial t} + \frac{\partial \Gamma_{e,x}}{\partial x} + \frac{\partial \Gamma_{e,y}}{\partial y} = -\beta_{ei} n_i n_e \tag{5}$$

$$\frac{\partial^2 \varphi}{\partial x^2} + \frac{\partial^2 \varphi}{\partial y^2} = -\frac{e}{\varepsilon_0}(n_i - n_e) \tag{6}$$

In Eqs. (4–6), n_i and n_e are the ion and electron densities, β_{ei} is the electron-ion recombination rate coefficient, and φ is the potential. The coordinate axes are shown in Figs. 2 and 3. The x and y components of ion and electron fluxes are

$$\begin{aligned} \Gamma_{i,x} &= -D_i \frac{\partial n_i}{\partial x} + \mu_i n_i E_x + n_i u_{\text{flow}}(y), \\ \Gamma_{i,y} &= -D_i \frac{\partial n_i}{\partial y} + \mu_i n_i E_y \end{aligned} \tag{7}$$

$$\begin{aligned} \Gamma_{e,x} &= -D_e \frac{\partial n_e}{\partial x} - \mu_e n_e E_x + n_e u_{\text{flow}}(y), \\ \Gamma_{e,y} &= -D_e \frac{\partial n_e}{\partial y} - \mu_e n_e E_y \end{aligned} \tag{8}$$

where μ_i and μ_e are the ion and electron mobilities, D_i and D_e are the diffusion coefficients $D_i/\mu_i = D_e/\mu_e = k_B T/e$, $\boldsymbol{E} = -\nabla\varphi$ is the electric field, and $u_{\text{flow}}(y)$ is the flow velocity profile in the test section, assumed to be uniform. The electron and ion mobilities are taken from [33]:

$$\mu_i = \frac{1.45 \times 10^3}{p^*} \frac{\text{cm}^2}{\text{V}\cdot\text{s}}, \quad \mu_e = \frac{4.4 \times 10^5}{p^*} \frac{\text{cm}^2}{\text{V}\cdot\text{s}}, \quad p^* = p(\text{torr}) \frac{300}{T} \tag{9}$$

The initial conditions assume quasi-neutral plasma ($n_e = n_i$). The cathode and the anode are extending from $x = 0$ to $x = L$ and from $x = L/4$ to $x = 3L/4$, respectively, where L is the length of the computational domain, 13.6 cm long and 1.5 cm wide. The system of Eqs. (4–6) is solved with the following boundary conditions:

$$x = 0, 1: \ \frac{\partial n_i}{\partial x} = \frac{\partial n_e}{\partial x} = \frac{\partial \varphi}{\partial x} = 0 \tag{10}$$

$$y = 0: \ \frac{\partial n_i}{\partial y} = 0, \qquad n_e = 0, \qquad \varphi = 0 \tag{11}$$

$$\begin{aligned} &y = 1, \qquad L/4 \le x \le 3L/4: \ n_i = 0, \frac{\partial n_e}{\partial y} = 0, \varphi = U \\ &0 \le x \le L/4 \quad \text{and} \quad 3L/4 \le x \le 1: \ \frac{\partial n_i}{\partial y} = \frac{\partial n_e}{\partial y} = \frac{\partial \varphi}{\partial y} = 0 \end{aligned} \tag{12}$$

Basically, the model describes electron and ion removal from the initially quasi-neutral plasma moving in the positive x direction at the flow velocity by the applied electric field, which does not produce additional ionization in the flow. The system of Eqs. (4–6) is solved using a nonlinear stiff partial differential equation solver PDETWO [34].

IV. Results and Discussion

The experiments have been conducted in three different fuel/oxidizer mixtures at near stoichiometric conditions, ethylene/dry air, ethylene/20%O_2/80%Ar mixture, and propane/20%O_2-80%Ar mixture. In all three cases, the pressure in the combustor (stagnation pressure) before ignition was $P_0 = 310$–325 torr. Steady flame, ignited by the spark plugs and stabilized by the flame holder, was obtained only in one of these mixtures: ethylene/oxygen/argon. In the other two mixtures, the flame was unstable and was repeatedly blown off by the flow entering the combustor ($u \sim 30$ m/s) and reignited as long as the spark plugs were operating. Under these conditions, turning the spark plugs off resulted in the flame extinguishing. In an ethylene–air flow, unsteadiness occurs because of a lower flame temperature due to a higher specific heat of nitrogen compared with that of argon. In a propane–oxygen–argon flow, the unstable flame behavior is due to a longer propane ignition delay time compared with that of ethylene [35]. In all three cases, the run time did not exceed several seconds to prevent overheating of the combustor, which was not actively cooled.

The mass flow rate of a baseline stoichiometric ethylene/oxygen/argon mixture, determined from Eq. (3) using plenum conditions before ignition ($\gamma = 1.51$, $R = 220$ J/kg·K, $P_0 = 321$ torr,

Table 1 Pressures before and after ignition in $C_2H_4/O_2/Ar$ mixture

	P_0, torr	P_1, torr	P_2, torr
Before ignition	325	12.0	22.0
After ignition	730	15.6	15.7

$T_0 = 300$ K), is $\dot{m} = 9.6$ g/s. After ignition, the steady-state stagnation pressure in the combustor increases due to a higher stagnation temperature at the same mass flow rate [see Eq. (3)]. Static pressures in the supersonic test section have been measured at two locations, at the nozzle exit P_1 and upstream of the diffuser inlet P_2, as shown in Fig. 2. Table 1 shows the stagnation and static pressures before and after ignition.

Combustion completeness was determined from the infrared absorption spectra of the combustion products sampled by a pitot probe in the supersonic test section (see Fig. 2). Figure 4 compares absorption spectra of the $C_2H_4/O_2/Ar$ mixture at the equivalence ratio of $\Phi = 0.95$ and of the combustion products at 0.25 cm^{-1} resolution, with and without ignition. From Fig. 4, it can be seen that the fuel (ethylene) has burned almost completely, whereas the concentrations of combustion products, CO, CO_2 and H_2O, considerably increased. This suggests that, at these conditions, the combustor (stagnation) temperature is close to the adiabatic flame temperature, $T_{ad} = 2620$ K, calculated for 18.75%O_2, 6.25%C_2H_4, and 75% Ar mixture at $P_0 = 1$ atm. At these conditions, the flow Mach number in the supersonic test section after ignition was estimated from the plenum-to-static pressure ratio using quasi-one-dimensional isentropic flow theory for a stoichiometric $C_2H_4/O_2/Ar$ mixture in chemical equilibrium at $T_0 = 2000$ K ($\gamma = 1.39$, $R = 221$ J/kg · K), $M = 3.16$. At a higher equivalence ratio, $\Phi = 1.13$, only about 60% of the fuel burns, and less CO, CO_2, and H_2O formed. Experiments also showed that the flame is more stable at near-stoichiometric conditions compared with the fuel-rich conditions.

Figure 5 shows UV/visible emission spectra of the $C_2H_4/O_2/Ar$ flame in the combustor at the conditions of Fig. 4 ($P_0 = 730$ torr, $\Phi = 0.95$). Emission from $CH(A^2\Delta - X^2\Pi)$ 430 nm bands, $C_2(A^3\Pi_g\text{-}X'^3\Pi_u)$ Swan bands, and $OH(A^2\Sigma^+\text{-}X^2\Pi)$ 306.4 nm bands, as well as H atom line at 656 nm and O atom line at 777 nm, were detected at these conditions. Emission spectra from the supersonic test section also showed presence of the same species, although the signal-to-noise here was significantly lower because of the lower flow density than in the combustor (by about a factor of 15). No emission from electronically excited CO was detected either in plenum or in the supersonic test section.

The R branch of the partially rotationally resolved $CH(A^2\Delta\text{-}X^2\Pi)$ emission spectra, (0,0) and (1,1) bands, has been used to infer the flame temperature at these conditions. This method has been previously used to infer hydrocarbon flame temperatures [36,37]. In particular, analysis of high-resolution CH emission spectra [37] showed no evidence of self-absorption, which may considerably affect the temperature value inferred from partially resolved spectra. Spectroscopic constants of CH molecule and rotational energy levels are taken from [38]. The rotational line intensities are taken from [39]. Figure 6 shows the experimental CH spectrum of Fig. 5 with the synthetic spectrum calculated at the rotational temperature of $T_0 = 2000$ K. It can be seen that the two spectra in Fig. 6 are on top of each other, except for a portion of a P branch. The flame temperature inferred from comparison of the two spectra is $T_0 = 2000 \pm 200$ K, which is somewhat lower than the adiabatic flame temperature at these conditions, $T_{ad} = 2620$ K. The lower temperature value inferred from the CH spectrum may be due to heat transfer to the combustor walls and also possibly due to continuing combustion downstream of the plenum, in the converging part of the nozzle (see Figs. 2 and 3). Based on the inferred stagnation temperature value, the static temperature in the supersonic test section (at $M = 3.16$) is $T = 670 \pm 70$ K (assuming isentropic flow at $\gamma = 1.39$). UV/visible emission spectra measured in ethylene/dry air flows (at the unsteady combustion conditions) also showed presence of CH, C_2, and OH, as well as O and H atoms. No emission from electronically excited nitrogen, CO, or NO was detected.

In the present experiments, ionization in the combustion chamber is created by chemi-ionization reactions in the hydrocarbon flame, such as a well-known reaction [13–16,40,41]

$$CH + O \rightarrow CHO^+ + e^- \tag{13}$$

When no voltage is applied to the electrode placed in the supersonic test section (see Sec. II), the ionized combustion product flow remains quasi neutral. When dc voltage is applied to the electrodes, both the electrons and the ions are removed from the flow by the applied field, although electrons are removed faster because of their higher mobility. This generates electrical current and creates a positive space charge between the electrodes. Note that as long as the applied voltage is lower than the breakdown voltage, the induced current measured between the biased electrode and the grounded test section is entirely due to the removal of charged species (electrons

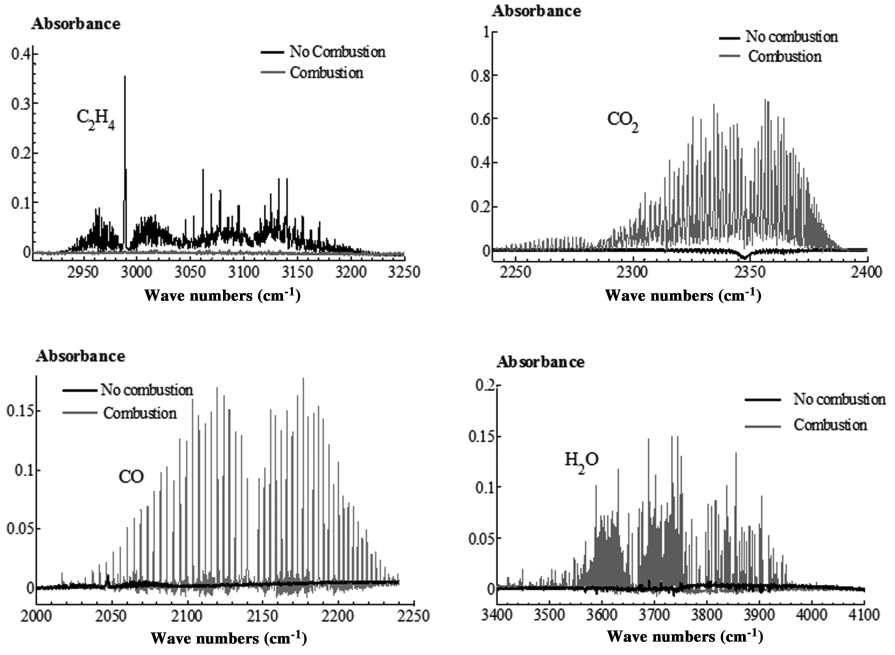

Fig. 4 Infrared absorption spectra of the $C_2H_4/O_2/Ar$ mixture with and without combustion. $\Phi = 0.95$, $P_0 = 730$ torr.

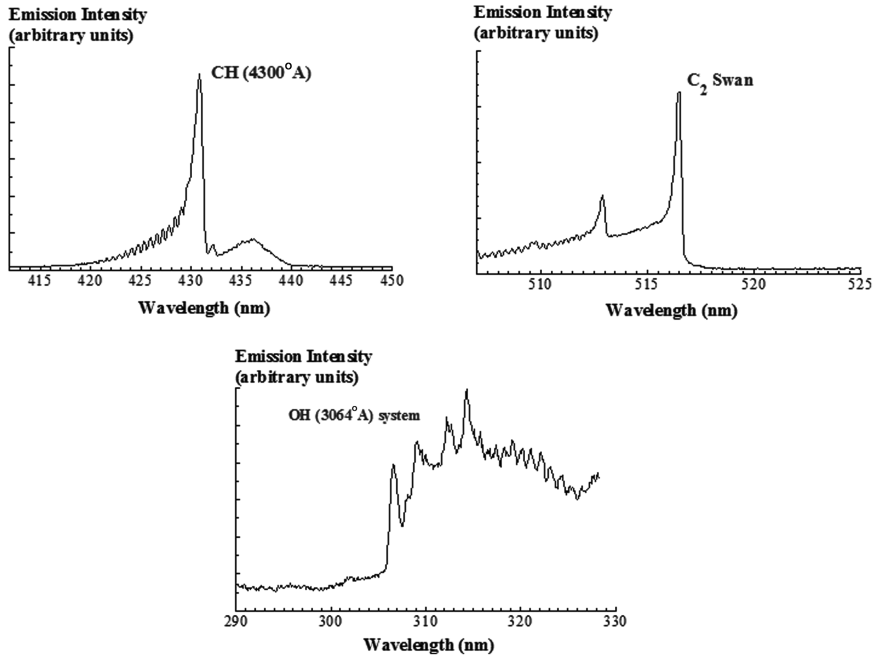

Fig. 5 UV/visible emission spectra of the $C_2H_4/O_2/Ar$ mixture at $\Phi = 0.95$, $P_0 = 730$ torr.

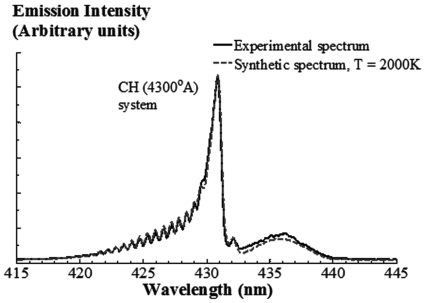

Fig. 6 Experimental and best fit synthetic CH spectra at the conditions of Fig. 5. Best fit combustor temperature is $T_0 = 2000 \pm 200$ K.

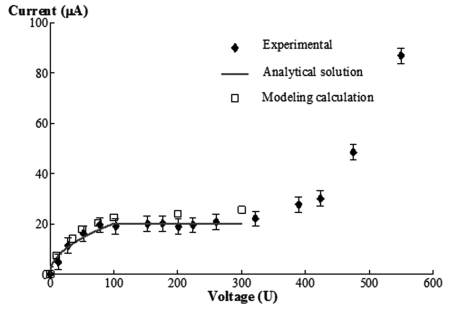

Fig. 7 Current-voltage characteristic of Thomson discharge in the $M = 3$ test section. $C_2H_4/O_2/Ar$ mixture, $\Phi = 1$, $P_0 = 730$ torr. Uncertainty in current measurements is ± 2 μA.

and ions) from the ionized flow. In other words, the applied field does not produce any ionization, and the current is sustained by chemi-ionization in the nozzle plenum. This type of a non-self-sustained electric discharge is known as Thomson discharge [10].

When the applied voltage is sufficiently high (but still below the breakdown threshold), the electrons are removed from the supersonic ionized flow at the same rate they are brought to the test section by the flow, resulting in current saturation. Basically, the saturation current is equal to the flux of electrons through the test section. Therefore, at saturation, the electron density in the flow can be inferred from the current,

$$I_{\text{sat}} = en_e A_{\text{cross}} u_{\text{flow}} \tag{14}$$

where I_{sat} is the saturation current, e is the elementary charge, n_e is electron density, $A_{\text{cross}} = 6.2$ cm^2 is the cross-sectional area of the flow, and $u_{\text{flow}} = M\sqrt{\gamma RT} = 1450 \pm 70$ m/s is the flow velocity in the test section. Similar methods of electron production rate and electron density measurements have been previously used in optically pumped plasmas [10–12] and in hydrocarbon flames [42,43]. Further increase of the voltage results in electrical breakdown (i.e., additional ionization by the applied field), which dramatically increases the current. In the present experiments, the voltage was kept below the breakdown threshold, and current voltage characteristic of the Thomson discharge was measured up to the breakdown point.

Figure 7 shows a typical current-voltage characteristic measured in a flow of $C_2H_4/O_2/Ar$ combustion products at $P_0 = 1$ atm and $\Phi = 1$. In Fig. 7, three different discharge regimes (current rise, saturation, and breakdown) can be clearly identified. A well-pronounced saturation plateau at $U_e = 100$–300 V demonstrates that nearly all electrons are removed from the flow long before breakdown occurs at $U_e \sim 500$ V. This shows that at $U_e < 300$ V, electron impact ionization does not contribute to the measured current. Figure 7 also shows a current-voltage characteristic predicted by the kinetic model described in Sec. III at $n_e = 10^8$ cm^{-3}, as well as an analytic current-voltage characteristic obtained from a one-dimensional Thomson discharge theory [10],

$$\begin{aligned} I_e &= \left(\frac{4\varepsilon_0 \mu_i A}{h^3} I_{\text{sat}}^3\right)^{1/4} U_e^{1/2} = I_{\text{sat}} \left(\frac{U}{U_{\text{sat}}}\right)^{1/2}, \qquad U_e \le U_{\text{sat}}, \\ I_e &= I_{\text{sat}}, \qquad U_e > U_{\text{sat}} \end{aligned} \tag{15}$$

where

$$U_{\text{sat}} = \left(\frac{I_{\text{sat}} h^3}{4\varepsilon_0 \mu_i A}\right)^{1/2} \tag{16}$$

is the saturation voltage, ε_0 is the dielectric permeability of vacuum, μ_i is the ion mobility, $A = 27$ cm^2 is the electrode surface area, and h is the distance between the electrodes (test-section height). From Eq. (16), for $I_{\text{sat}} = 20 \pm 2$ μA (see Fig. 7), the saturation voltage is $U_{\text{sat}} = 100 \pm 15$ V. From Fig. 7, it can be seen that both numerical and analytic current-voltage characteristics are in good agreement

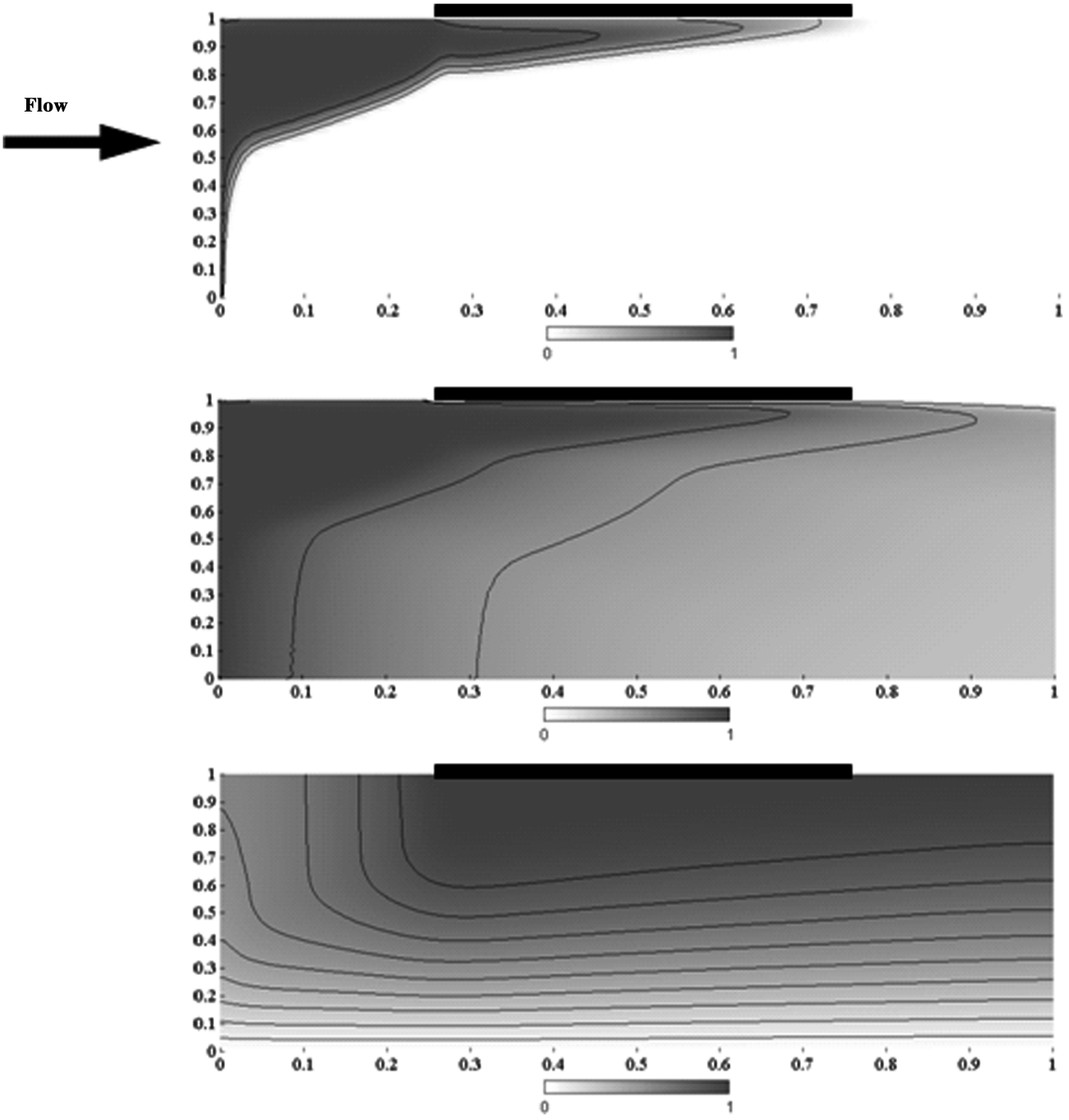

Fig. 8 Contour plots of electron density, ion density, and electrical potential in the supersonic test section at the saturation conditions.

with the experiment. From Eq. (14), for $I_{\text{sat}} = 20 \pm 2\ \mu\text{A}$, the electron density in the supersonic test section is $n_e = 1.4 \pm 0.2 \cdot 10^8\ \text{cm}^{-3}$, the ionization fraction is $n_e/N = (0.65 \pm 0.15) \cdot 10^{-9}$, and the electron flux through the test section is $S = I_{\text{sat}}/e = (1.25 \pm 0.13) \cdot 10^{14}$ electrons/s.

Using the quasi-one-dimensional isentropic compressible flow theory and assuming that the ionization fraction remains constant during the supersonic expansion, one can calculate the electron density in the combustor, $n_{e0} = 2.2 \cdot 10^9\ \text{cm}^{-3}$. This assumption is justified because, at this low electron density, the characteristic electron recombination time at the plenum conditions $\tau_{\text{rec}} = (\beta_{\text{ei}} \text{n}_{e0})^{-1} \sim 5$ ms is much longer than the nozzle expansion time $\tau_{\text{flow}} \sim u_{\text{flow}}/l \sim 100$. Here $\beta_{\text{ei}} \sim 10^{-7}\ \text{cm}^3/\text{s}$ is the electron-ion recombination rate and $l = 17$ cm is the nozzle length. This estimate shows that in high-speed, weakly ionized flows, where $\tau_{\text{flow}} \ll \tau_{\text{rec}}$, ionization equilibrium may not be established, and the electron density at these conditions may be far from its equilibrium value.

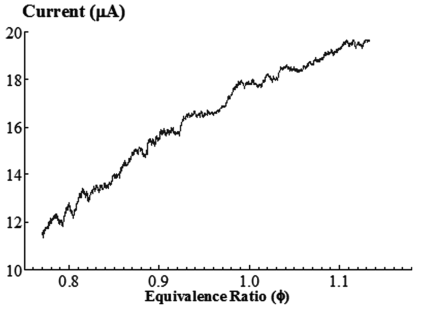

Fig. 9 Saturation current in the $M = 3$ flow of $C_2H_4/O_2/Ar$ combustion products as a function of the equivalence ratio; $P_0 = 730$ torr.

Indeed, the inferred value of the combustor electron density is more than an order of magnitude higher than the electron density for the stoichiometric $C_2H_4/O_2/Ar$ mixture at thermochemical equilibrium at the adiabatic flame temperature of $T_{ad} = 2620$ K, $n_{e0} = 5 \cdot 10^7$ cm^{-3}. Also, the electron density in the combustor exceeds the equilibrium value at the experimentally measured combustor temperature $T_0 = 2000 \pm 200$ K by several orders of magnitude. This demonstrates that the electron density in the $C_2H_4/O_2/Ar$ flame at the present conditions is much higher than its equilibrium value.

The aforementioned ionization measurements demonstrate how the Thomson probe, placed in the supersonic flow of combustion products, can be used for straightforward measurements of electron density in the flow, without affecting the flame by the applied electric field. Also, these results show that nearly all electrons can be removed from the combustion products flow by applying a modest electric field. This is further illustrated by the results of modeling calculations using the Thomson discharge model described in Sec. III. Figure 8 shows contour plots of electron and ion density, as well as of the electric potential in the supersonic test section. In Fig. 8, the flow pressure, temperature, and velocity are the same as inferred from the experimental data, the incident electron density is $n_e = 10^8$ cm^{-3} and the electrode voltage is $U_e = 100$ V. From Fig. 8, it can be seen that the electrons are indeed completely removed from the flow. Note that the ionization fraction at the present conditions is comparable with ionization fraction in the optical pumping experiment [7], in which removal of electrons from the plasma significantly affected UV/visible emission.

Measurements of the Thomson discharge saturation current while varying the equivalence ratio in the combustion chamber showed that the current (i.e., the electron density in the flow) is approximately proportional to the equivalence ratio (see Fig. 9). This suggests that measuring chemi-ionization current in the flow of combustion products can be used to monitor and control the equivalence ratio in the combustion chamber, especially at lean conditions or low combustion pressures, when the flame may become unstable.

This conclusion is further supported by the time-resolved flame emission and chemi-ionization current measurements at the unstable combustion conditions, in stoichiometric ethylene/dry air and propane/oxygen/argon mixtures. In these cases, the spark plugs remained on during the entire run, while we simultaneously monitored the flame emission from the combustor (CH 430 nm band at 431 nm and $C_2(0 \rightarrow 0)$ Swan band at 516 nm) and the chemi-ionization current in the supersonic test section. The results plotted in Fig. 10 show that chemi-ionization current spikes are in very good correlation with the CH emission spikes, which appear due to repeated ignition and flame blowoff in the combustor. A very similar correlation was detected between the current and the C_2 emission. Note that the chemi-ionization current spikes are not related to the spark plug current, which remains steady during the entire run. Again, this suggests that chemi-ionization current can be used both as a flame sensor and as a control parameter for feedback combustion control. Basically, current reduction would indicate approaching flame extinction, which can be countered by either adding more fuel to the combustor or by turning on an ignition source.

To detect the possible effect of electrons on the visible emission from the supersonic flow of combustion products, we measured time-resolved emission intensity of the CH 430 nm band system and of the $C_2(0 \rightarrow 0)$ Swan band (516 nm) in the $M = 3$ flow of $C_2H_4/O_2/Ar$ combustion products, with and without saturation voltage $U_{sat} = 200$ V applied to the electrodes. As discussed earlier, applying saturation voltage to the electrodes results in electron removal from the flow. Figure 11 shows the emission signal and the chemi-ionization current at these conditions. If the presence of electrons indeed affects the number densities of electronically excited $CH(A^2\Delta)$ and $C_2(A^3\Pi_g)$ states, suddenly turning the voltage on and off (and thereby changing the electron density) would result in a sudden change in emission intensity. However, one can see that the results of Fig. 11 show no detectable effect of applied voltage on CH and C_2 emission, respectively. Basically, this demonstrates that

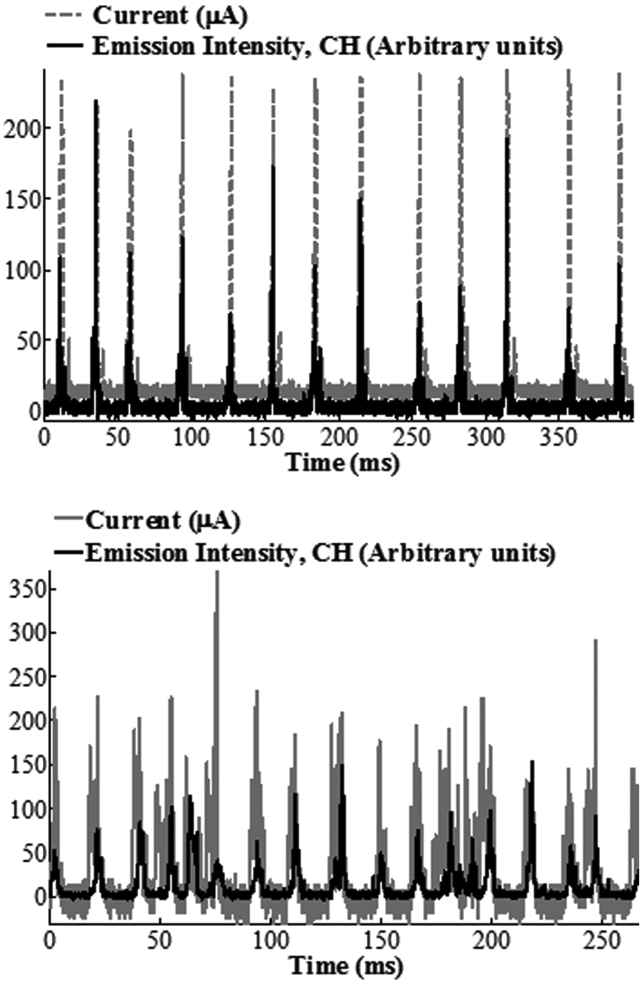

Fig. 10 Time-resolved flame emission from the combustor (CH, 431 nm) and chemi-ionization current in the $M = 3$ flow. Top, stoichiometric propane/oxygen/argon mixture; bottom, stoichiometric ethylene/dry air mixture.

formation of these electronically excited radiating species is not affected by chemi-ionization and energy transfer by electrons.

In a separate series of experiments, we injected one of the dominant species detected in emission of high-altitude rocket plumes, nitric oxide, 1) into the $M = 3$ flow of $C_2H_4/O_2/Ar$ combustion products in the supersonic test section using a pitot tube (see Fig. 2), and 2) into the subsonic $C_2H_4/O_2/Ar$ combustion product flow downstream of combustor using a stagnation pressure port (see Fig. 2). For both injection schemes, electronically excited states of NO and CN are generated by energy transfer from excited species in the combustion products flow. Figure 12 shows a photograph of a bow shock in front of the pitot probe, formed by a counterflow injection of a 5% NO/95% Ar mixture into the $M = 3$ flow. The emission intensity near the probe is higher because of the higher flow density behind the bow shock. Figure 13 shows the time-resolved NO emission signal, NO β band $(0 \rightarrow 10)$ at 358 nm, at these conditions. In Fig. 13, NO injection starts at $t = 3.2$ s and ends at $t = 8.0$ s. During this experiment, applying saturation voltage to the Thomson electrodes $U_{sat} = 200$ V did not result in detectable NO emission intensity change.

Because the NO emission signal-to-noise during supersonic injection was rather low due to a small NO fraction in the flow, we have done additional measurements using subsonic injection of NO/Ar and NO/N_2 mixtures (NO mole fraction in the flow is 0.5–1.0%). Subsonic NO injection resulted in considerable emission reduction from OH, CH, and C_2 in the $M = 3$ flow. Figure 14 shows low-resolution UV/visible emission spectra of the $M = 3$ flow in the test section, with and without the subsonic NO/Ar injection. Two NO β bands, $(0 \rightarrow 9)$ at 338 nm and $(0 \rightarrow 10)$ at 358 nm, as well as

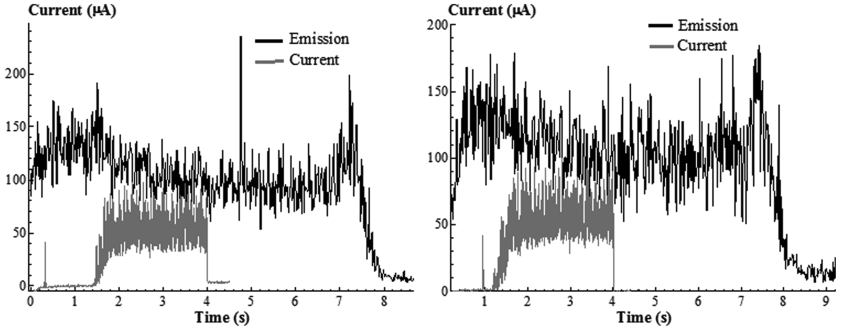

Fig. 11 Emission intensity (left, CH; right, C2) and saturation current ($U_{sat} = 200$ V) in $M = 3$ flow of $C_2H_4/O_2/Ar$ combustion products.

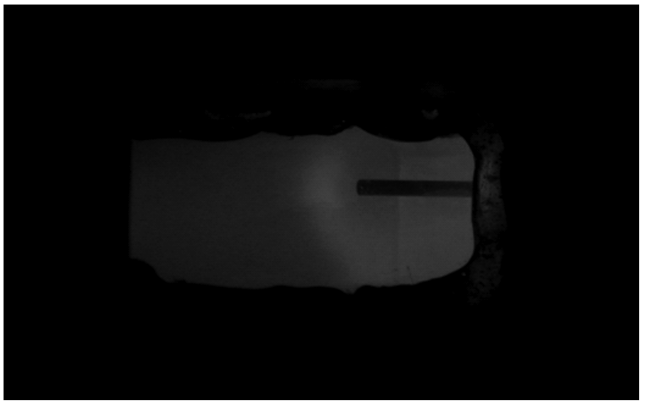

Fig. 12 Photograph of a bow shock formed in front of the pitot probe when an NO/Ar mixture is injected into the $M = 3$ flow of $C_2H_4/O_2/Ar$ combustion products; $\Phi = 1.0$, $P_0 = 730$ torr.

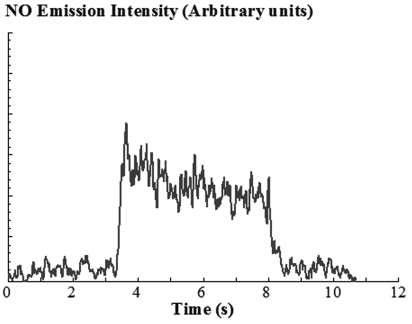

Fig. 13 Time-resolved NO emission signal, NO β band ($0 \rightarrow 10$) at 358 nm. $C_2H_4/O_2/Ar$ mixture with and without supersonic NO injection. Injection starts at $t = 3.2$ s and ends at $t = 8.0$ s; $\Phi = 1.0$, $P_0 = 730$ torr.

CN violet bands system at 388 nm, can be clearly identified when NO is injected. At these conditions, the possible effect of electrons on NO and CN emission from the $M = 3$ flow was again tested using the Thomson probe, as discussed previously. Figure 15 shows UV/visible emission spectra (OH, NO β, and CN violet bands) taken from an $M = 3$ combustion product flow with subsonic NO/Ar injection, with and without electrons present in the flow. It can be seen that removal of electrons from the flow by applying saturation Thomson voltage of $U_{sat} = 200$ V did not produce a detectable change in the UV/visible emission intensity, and so the two emission spectra in Fig. 15 basically coincide with each other. The same negative result was obtained with NO/N_2 injection: one can see that the spectra with and without electrons coincide again. This result, which is similar to the data obtained for CH and C_2 emission from the combustion product flow without NO injection (see Fig. 11), suggests that formation of electronically excited OH, NO, and CN is also unaffected by chemi-ionization and energy transfer by electrons.

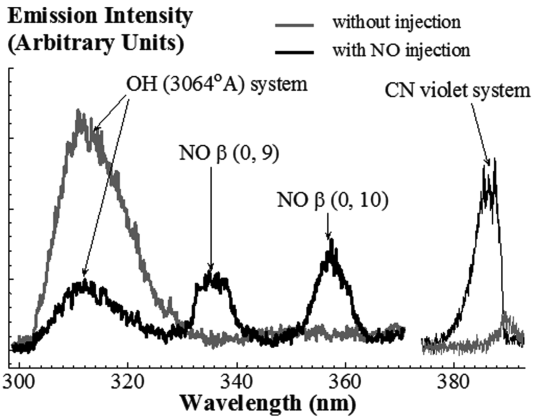

Fig. 14 UV/visible emission spectra from the $M = 3$ combustion product flow. $C_2H_4/O_2/Ar$ mixture with and without subsonic NO injection; $\Phi = 1.0$, $P_0 = 730$ torr.

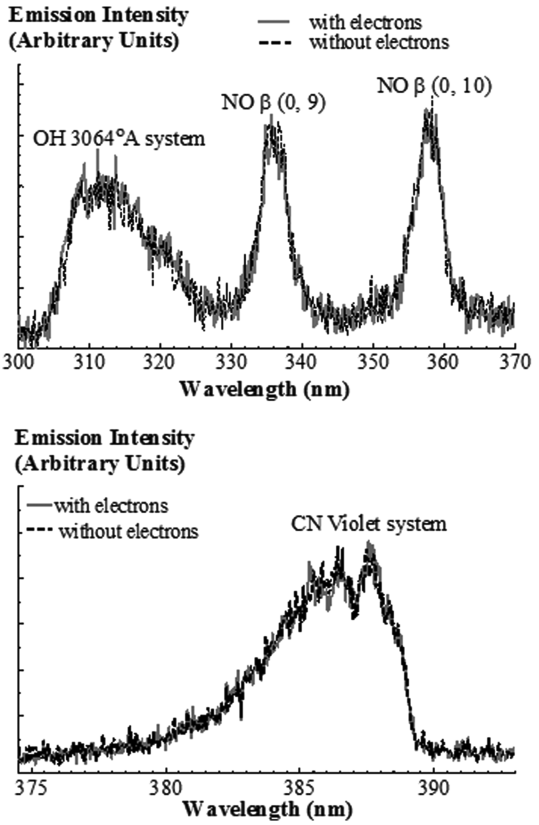

Fig. 15 UV/visible emission spectra (OH, NO β, and CN violet bands) in an $M = 3$ combustion product flow with subsonic NO injection, with and without electrons.

V. Summary

In the present experiments, a stable $C_2H_4/O_2/Ar$ flame is sustained and nearly complete combustion is achieved in a combustion chamber of an $M = 3$ supersonic nozzle, at a stagnation pressure of $P_0 = 1$ atm. UV/visible emission from CH (430 nm system), C_2 (Swan bands), and OH (306.4 nm system) is detected from both the combustion chamber and from the $M = 3$ flow of combustion products. Temperature in the combustor is inferred from the CH emission spectrum, $T_0 = 2000 \pm 200$ K. Electron density measured in the $M = 3$ flow of combustion products using the Thomson discharge is $n_e = 1.4 \pm 0.2 \cdot 10^8$ cm^{-3}, at the ionization fraction of $n_e/N = (0.65 \pm 0.15) \cdot 10^{-9}$. This corresponds to the electron density in the combustor of $n_{e0} = 2.2 \cdot 10^9$ cm^{-3}, which is more than an order of magnitude greater than the equilibrium electron density at the adiabatic flame temperature of $T_{ad} = 2620$ K. The chemi-ionization current measured in the $M = 3$ flow is proportional to the equivalence ratio in the combustor. The time-resolved chemi-ionization current is also found to be in very good correlation with the visible emission (CH and C_2 bands) from ethylene–air and propane–oxygen–argon flames in the combustor at the unstable combustion conditions. This suggests the possibility of developing a combustion sensor/feedback controller based on monitoring the chemi-ionization current.

The results also show that nearly all electrons can be removed from the supersonic flow of combustion products by applying a moderate transverse electric field. No effect of electron removal on emission from CH (430 nm) and C_2 (Swan band, 516 nm) has been detected. A similar result was obtained for OH (306.4 nm system), NO β bands, and CN violet band emission, when NO/Ar and NO/N_2 mixtures were injected into the combustion product flow. This suggests that formation of these electronically excited radiating species is unaffected by chemi-ionization and energy transfer by electrons. Ongoing and future work includes further measurements of coupling between chemi-ionization and chemiluminescence in combustion product flows, as well as feasibility studies of feedback combustion control, using chemi-ionization current as a control parameter.

Acknowledgment

The authors would like to acknowledge the continuing support of the Space Power and Propulsion Directorate of the U.S. Air Force Office of Scientific Research (AFOSR grant FA9550-05-1-0024).

References

[1] Simmons, F. R., *Rocket Exhaust Plume Phenomenology*, Aerospace Press, El Segundo, 2000.

[2] Blanc, A., Deimling, L., and Eisenreich, N., "Radiation Emitted from Rocket Plumes," *Propellants, Explosives, Pyrotechnics*, Vol. 22, No. 3, 1997, pp. 152–155. doi:10.1002/prep.19970220310

[3] Blanc, A., Deimling, L., and Eisenreich, N., "UV and IR Signatures of Rocket Plumes," *Propellants, Explosives, Pyrotechnics*, Vol. 27, No. 3, 2002, pp. 185–189. doi:10.1002/1521-4087(200206)27:3<185::AID-PRE-P185>3.0.CO;2-H

[4] Hudson, M. K., and Shanks, R. B., "UV, Visible, and Infrared Spectral Emissions in Hybrid Rocket Plumes," *International Journal of Turbo and Jet Engines*, Vol. 15, No. 1, 1998, pp. 71–87.

[5] Romanovsky, Yu., Alpatov, V., Platov, Yu., Chernouss, S., Kosch, M., and Steen, A., "Optical Investigations in the "ERLE" Project," *Physics and Chemistry of the Earth, Part B: Hydrology, Oceans and Atmosphere*, Vol. 25, Nos. 5–6, 2000, pp. 503–506. doi:10.1016/S1464-1909(00)00053-8

[6] Platov, Yu. V., Kulikova, G. N., and Chernouss, S. A., "Classification of Gas-Dust Structures in the Upper Atmosphere Associated with the Exhausts of Rocket-Engine Combustion Products," *Cosmic Research* (Translation of Kosmicheskie Issledovaniya), Vol. 41, No. 2, 2003, pp. 153–158. doi:10.1023/A:1023335014306

[7] Plönjes, E., Palm, P., Rich, J. W., Adamovich, I. V., and Urban, W., "Electron-Mediated Vibration-Electronic (V-E) Energy Transfer in Optically Pumped Plasmas," *Chemical Physics*, Vol. 279, No. 1, 2002, pp. 43–54. doi:10.1016/S0301-0104(02)00387-7

[8] Utkin, Yu. G., Adamovich, I. V., and Rich, J. W., "Time-Resolved Measurements of Ionization and Vibration-to-Electronic Energy Transfer in Optically Pumped Plasmas," *Journal of Physics D: Applied Physics*, Vol. 38, No. 5, 2005, pp. 688–696. doi:10.1088/0022-3727/38/5/005

[9] Plonjes, E., Palm, P., Chernukho, A. P., Adamovich, I. V., and Rich, J. W., "Time-Resolved Fourier Transform Infrared Spectroscopy of Optically Pumped Carbon Monoxide," *Chemical Physics*, Vol. 256, No. 3, 2000, pp. 315–331. doi:10.1016/S0301-0104(00)00096-3

[10] Adamovich, I. V., Saupe, S., Grassi, M. J., Schulz, O., Macheret, S., and Rich, J. W., "Vibrationally Stimulated Ionization of Carbon Monoxide in Optical Pumping Experiments," *Chemical Physics*, Vol. 173, No. 3, 1993, pp. 491–504. doi:10.1016/0301-0104(93)80163-4

[11] Ploenjes, E., Palm, P., Adamovich, I. V., and Rich, J. W., "Ionization Measurements in Optically Pumped Discharges," *Journal of Physics D: Applied Physics*, Vol. 33, No. 16, 2000, pp. 2049–2056. doi:10.1088/0022-3727/33/16/317

[12] Palm, P., Plönjes, E., Buoni, M., Subramaniam, V. V., and Adamovich, I. V., "Electron Density and Recombination Rate Measurements in CO-Seeded Optically Pumped Plasmas," *Journal of Applied Physics*, Vol. 89, No. 11, 2001, pp. 5903–5910. doi:10.1063/1.1359754

[13] Calcote, H. F., "Nonequilibrium Ionization in Flames," *ARS Ions in Flames and Rocket Exhausts Conference*, Vol. 12, Progress in Astronautics and Aeronautics, Academic, New York, 1963, pp. 107–144.

[14] Sugden, T. M., "Survey of Flame Ionization Work at the University of Cambridge," *ARS Ions in Flames and Rocket Exhausts Conference*, Vol. 12, Progress in Astronautics and Aeronautics, Academic, New York, 1963, pp. 145–164.

[15] Smith, F. T., and Gatz, C. R., "Chemistry of Ionization in Rocket Exhausts," *ARS Ions in Flames and Rocket Exhausts Conference*, Vol. 12, Progress in Astronautics and Aeronautics, Academic, New York, 1963, pp. 301–316.

[16] Pergament, H. S., and Calcote, B. F., "Thermal and Chemi-Ionization Processes in Afterburning Rocket Exhausts," *11th Symposium (International) on Combustion*, Vol. 11, No. 1, Elsevier, New York, 1967, pp. 597–611.

[17] Becker, K. H., and Bayes, K. D., "CO Chemiluminescence from Flames," *Journal of Chemical Physics*, Vol. 48, No. 2, 1968, pp. 653–661. doi:10.1063/1.1668696

[18] Shackleford, W. L., and Mastrup, F. N., "Excitation and Quenching of CO Fourth Positive Chemiluminescence due to Reactions Involving C_2O^*," *Journal of Chemical Physics*, Vol. 57, No. 9, 1972, pp. 3933–3944. doi:10.1063/1.1678865

[19] Marmo, F. F., Padur, J., and Warneck, P., "Vacuum-Ultraviolet Chemiluminescence in the Reaction of Atomic Oxygen with Acetylene," *Journal of Chemical Physics*, Vol. 47, No. 4, 1967, p. 1438. doi:10.1063/1.1712099

[20] Fontijn, A., Ellision, R., Smith, W. H., and Hesser, J. E., "Chemiluminescent Emission of CO Fourth Positive Bands in Nitrogen Atom/Oxygen Atom/Reactive Carbon Compound Systems. Relation to Chemi-Ionization," *Journal of Chemical Physics*, Vol. 53, No. 7, 1970, pp. 2680–2687. doi:10.1063/1.1674391

[21] Fontijn, A., and Vree, P. H., "Catalyzed Enhancement of Chemi-Ionization in Atomic Nitrogen and Oxygen Mixtures," *Journal of Physical Chemistry*, Vol. 70, No. 6, 1966, p. 2071. doi:10.1021/j100878a518

[22] Fontijn, A., and Johnson, S. E., "Mechanism of CO Fourth Positive VUV Chemiluminescence in the Atomic Oxygen Reaction with Acetylene. Production of $C(^3P, ^1D)$," *Journal of Chemical Physics*, Vol. 59, No. 12, 1973, pp. 6193–6200. doi:10.1063/1.1679998

[23] Fontijn, A., Gourmi, A., and Brock, P. E., "Pressure-Dependence of the $CO(d^3\Delta\text{-}a^3\Pi)$ Triplet Bands Chemiluminescence Intensities from the $O + C_2H_2$ Reaction: Mechanistic Implications," *Combustion and Flame*, Vol. 121, No. 4, 2000, pp. 699–701. doi:10.1016/S0010-2180(00)00100-0

[24] Fontijn, A., Fernandez, A., Ristanovic, A., Andall, M. Y., and Jankowiak, J. T., "CO Chemiluminescence and Kinetics of the $C_2 + O_2$ Reaction," *Journal of Physical Chemistry A*, Vol. 105, No. 13, 2001, pp. 3182–3189. doi:10.1021/jp003529r

[25] Becker, K. H., Kley, D., and Norstrom, R. J., "OH* Chemiluminescence in Hydrocarbon Atom Flames," *12th Symposium (International) on Combustion*, Vol. 12, No. 1, Elsevier, New York, 1969, pp. 405–413.

[26] Pearse, R. W. B., and Gaydon, A. G., *Identification of Molecular Spectra*, 4th ed., Chapman and Hall, London, 1976.

[27] Devriendt, K., and Peeters, J., "Direct Identification of the $C_2H(X^2\Sigma^+) + O(^3P) \rightarrow CH(A^2\Delta) + CO$ Reaction as the Source of the $CH(A^2\Delta \rightarrow X^2\Pi)$ Chemiluminescence in $C_2H_2/O/H$ Atomic Flames," *Journal of Physical Chemistry A*, Vol. 101, No. 14, 1997, pp. 2546–2551.

[28] Muruganandam, T. M., Kim, B., Olsen, R., Patel, M., Romig, B., and Seitzman, J. M., "Chemilumemiscence Based Sensors for Turbine Engines," *39th AIAA/ASME/SAE/ASEE Joint Propulsion Conference and Exhibit*, AIAA Paper 2003-4490, July 2003.

[29] Thiruchengode, M., Nair, S., Neumeier, Y., Lieuwen, T., Seitzman, J. M., and Zinn, B. T., "Active Control System for LBO Margin Reduction in Turbine Engines," *41st Aerospace Sciences Meeting and Exhibit*, AIAA Paper 2003-1008, Jan. 2003.

[30] Eriksson, L., and Nielson, L., "Ionization Current Interpretation for Ignition Control in Internal Combustion Engines," *Control Engineering Practice*, Vol. 5, No. 8, 1997, pp. 1107–1113. doi:10.1016/S0967-0661(97)00103-2

[31] Chorpening, B. T., Thornton, J. D., and Benson, K. J., "Flame Ionization Sensor Testing in a Pressurized Combustor," *IEEE Sensors 2005: 4th IEEE Conference on Sensors*, Institute of Electrical and Electronics Engineers, Piscataway, NJ, Oct.–Nov. 2005, pp. 987–990.

[32] Adamovich, I. V., "Control of Electron Recombination Rate and Electron Density in Optically Pumped Nonequilibrium Plasmas," *Journal of Physics D: Applied Physics*, Vol. 34, No. 3, 2001, pp. 319–325. doi:10.1088/0022-3727/34/3/312

[33] Surzhikov, S. T., and Shang, J. S., "Two-Component Plasma Model for Two-Dimensional Glow Discharge in Magnetic Field," *Journal of Computational Physics*, Vol. 199, No. 2, 2004, pp. 437–464.

[34] Madsen, N. K., and Sincovec, R. F., "Algorithm 540: PDECOL, General Collocation Software for Partial Differential Equations [D3]," *ACM Transactions on Mathematical Software*, Vol. 5, No. 3, 1979, p. 326. doi:10.1145/355841.355849

[35] Davidson, D. F., and Hanson, R. K., "Fundamental Kinetics Database Utilizing Shock Tube Measurements," Vol. 1, Mechanical Engineering Dept., Stanford Univ., Stanford, CA, 2005, http://navier.stanford.edu/hanson/publications/Fundamental%20Kinetics%20Database%20Volume%201.pdf.

[36] Barreta, L. G., da Rocha, C. J., Carinhana, D., Sbampato, M. E. Jr., de Oliveira, A. C., dos Santos, A. M., and dos Santos, L. R., "Emission Spectroscopy of CH Radical to Determine the Temperature of Ethanol Flame," *Proceedings of XXVI Brazilian National Meeting in Condensed Matter Physics*, Annals of Optics, Vol. 5, 2003.

[37] Carinhana, D., Barreta, L. G. Jr., da Rocha, C. J., dos Santos, A. M., and Bertran, C. A., "Determination of Gas Liquefied Petroleum Flame Temperatures Using Emission Spectroscopy," *Proceedings of XXIX Brazilian National Meeting in Condensed Matter Physics*, Annals of Optics, 2006.

[38] Huber, K. P., and Herzberg, G., *Molecular Spectra and Molecular Structure IV. Constants of Diatomic Molecules*, Van Nostrand Reinhold, New York, 1979.

[39] Kovacs, I., *Rotational Structure in the Spectra of Diatomic Molecules*, Elsevier, New York, 1969.

[40] Weinberg, F. J., *Advanced Combustion Methods*, Academic, London, 1986.

[41] Gaydon, A. G., and Wolfhard, H. G., *Flames: Their Structure, Radiation and Temperature*, Chapman and Hall, London, 1970.

[42] Lawton, J., and Weinberg, F., "Maximum Ion Currents from Flames and the Maximum Practical Effects of Applied Electric Fields," *Proceedings of Royal Society of London, Series A, Mathematical and Physical Sciences*, Vol. 277, No. 1371, 1964, pp. 468–497.

[43] Boothman, D., Lawton, J., Melinek, S. J., and Weinberg, F. J., "Rates of Ion Generation in Flames," *12th Symposium (International) on Combustion*, Vol. 12, No. 1, Elsevier, New York, 1969, pp. 969–978.